Sustainable Energy & Fuels

ROYAL SOCIETY OF CHEMISTRY

PAPER

View Article Online
View Journal | View Issue

Check for updates

Cite this: *Sustainable Energy Fuels*, 2025, **9**, 2079

Improving anion exchange membrane stability with hydrophilic polyethylene for advanced aqueous organic redox flow batteries†

Chenggang Li,‡[a] Mei Han,‡[b] Rui Han[a] and P. Chen *[b]

Received 10th December 2024
Accepted 20th February 2025

DOI: 10.1039/d4se01720j

rsc.li/sustainable-energy

Anion exchange membranes (AEMs) are a vital component of aqueous organic redox flow batteries (AORFBs). Conventional AEMs often suffer from high resistance and typically lack mechanical strength and durability, particularly when used over large areas. In this work, we report a high-performance combination membrane (CM) formed by the straightforward adhesion of a hydrophilic porous polyethylene (HPE) layer to an AEM. The exceptional hydrophilic stability of HPE in the electrolyte endows this CM with remarkable stability in single-cell operations. Furthermore, the CM effectively prevents electrolyte crossover while facilitating efficient anion transport, demonstrating long-term stability in a 52-stack battery, with each CM scaled up to an active area of 830 cm^2. This work presents a facile and scalable method for fabricating highly durable AEMs, offering significant advancements in the field of AORFBs.

Introduction

Redox flow batteries (RFBs) are rechargeable systems characterized by the decoupling of energy and power, where redox-active materials are dissolved in suitable solvents and pumped through the electrodes. RFBs represent one of the most promising technologies for stationary energy storage due to their scalability and flexibility.[1–4] They are anticipated to be in high demand driven by global climate initiatives, such as the European Green Deal, aiming to achieve zero release by leveraging intermittent energy sources.[5] To date, numerous flow battery systems have been developed, with the vanadium redox flow battery (VRFB) being the first to be industrialized and continuing to dominate the market.[6,7] Recently, organic redox flow battery (ORFB) systems have drawn extensive attention because of the ever-growing need for sustainable development. In particular, water-based aqueous organic redox flow batteries (AORFBs) are viewed as promising alternatives as they omit critical metals, aligning with eco-friendly energy storage solutions.[8,9] However, given the limited electrochemical stability window of water (~1.23 V), current research on AORFB development primarily focuses on synthesizing redox-active species that offer high solubility and stability to achieve enhanced energy density.[8,10] As another key component, the development of membranes is of equal importance. Unfortunately, even though a number of commercial membranes have been systematically studied, they all exhibit high resistance or severe capacity degradation, which significantly hinders their application in AORFBs.[11,12] Recently, considerable efforts have been focused on synthesizing suitable membranes that offer favorable conductivity and excellent performance.[13–19] For instance, Song *et al.* reported the development of intrinsically ultra-microporous anion exchange membranes (AEMs), with the optimized MTCP-50 AEM exhibiting superior conduction and stability in neutral AORFBs.[17] However, most studies have been conducted at the single cell level with small membrane areas (50 cm^2), and the stability of these membranes when scaled up to commercially viable areas has not been explored. This oversight may be due to the low mechanical strength and durability of these AEMs when used over large areas, which limits their practical application. Similarly, AEMs are also a core component in alkaline water electrolysis (AWE) technologies, where high mechanical strength and durability are essential.[20–23] While most previous studies have focused on improving the AWE performance of membranes at the single cell level, the operability of these membranes in stacked cells has been greatly overlooked.[24] Recently, Choi *et al.* reported a thin film composite (TFC) membrane consisting of an AEM and hydrophilic porous polyethylene (HPE). The dense and highly anion-conductive AEM layer effectively prevents electrolyte crossover while promoting anion transport. Additionally, the high tenacity and nanosized pores of the HPE support reinforce the mechanical properties, while its highly porous and thin structure reduces mass transport resistance across the TFC.

[a]*Key Laboratory of Innovation Centre for Organic Redox Flow Battery, Suqian Shidai Energy Storage Co., Ltd, Jiangsu, 211170, P. R. China*

[b]*Department of Chemical Engineering and Waterloo Institute of Nanotechnology, University of Waterloo, N2L 3G1, Canada. E-mail: p4chen@uwaterloo.ca*

† Electronic supplementary information (ESI) available. See DOI: https://doi.org/10.1039/d4se01720j

‡ These authors contributed equally to this work.

Consequently, these TFC membranes have significantly improved performance in both single unit cell and three-stack cell configurations in AWE.[25] This indicated to us that HPE should similarly be able to improve the performance of AEMs used in AORFBs.

In this work, we initially examine the physicochemical properties and battery performance of various commercial membranes alongside the MTCP-50 AEM in *N*,*N*,*N*-2,2,6,6-heptamethylpiperidinyl oxy-4-ammonium chloride (TEMPTMA) and methyl viologen dichloride (MV)-based AORFB systems, as detailed in Table S1.† The commercial membranes, when compared to the MTCP-50 AEM, display either lower ionic conductivity or severe capacity degradation. Consequently, we focus on a combination membrane (CM) based on the MTCP-50 AEM, which consists of the MTCP-50 AEM layer and HPE. This integration of HPE enables the CM to demonstrate enhanced stability and superior performance in both single cell and 52-stack cell configurations, with successful scaling up of the active CM area to 830 cm^2 in a single piece. Our findings present a facile and scalable approach to fabricate high-performance AEMs.

Experimental

Materials

Hydrophilic porous polyethylene (HPE) was purchased from Henan Chaoli New Energy Co., Ltd (China). Sodium chloride (NaCl) was purchased from Guoyao Co., Ltd (China). MTCP-50 anion exchange membranes (AEMs) were provided by Zhong ke & Shidai Energy Storage Co., Ltd (China). *N*,*N*,*N*-2,2,6,6-heptamethylpiperidinyl oxy-4-ammonium chloride (TEMPTMA) and methyl viologen dichloride (MV) were provided by Suqian Shidai Energy Storage Co., Ltd (China). Apart from the AEM, all chemicals and materials were utilized as received, without further purification.

Characterization

The ^1H NMR spectra were recorded on a Bruker 510 instrument (Germany) in DMSO-d_6 as the standard solvent to compare the chemical structure of the MTCP-50 AEMs before and after 1000 h cycles. The chemical functional groups and compositions of the MTCP-50 AEMs before and after 1000 h cycles were identified using FT-IR (Spectrum Two spectrometer, America). Scanning electron microscopy (SEM) was conducted on a JSM-6360LA microscope (Japan) to observe the surface morphology of HPE and MTCP-50. To measure the ohmic resistance of the cell, the electrochemical impedance spectroscopy (EIS) was performed on an electrochemical workstation (DH7000C, China). For the EIS tests, the frequency range is set from 100 mHz to 10 000 Hz at a constant current of 0.3 A. The high frequency resistance (HFR) at 1–2000 Hz in the Nyquist plot was selected for quantifying the ohmic resistance of the cell.

Ionic conductivity

The anion conductivity of the MTCP-50 AEM was measured in an H-type cell using an AC impedance analyzer (DH7000C, China). The diameter (D) of the connected circular hole and the thickness (L) of the AEM sample in Cl^- form were quickly measured using a graduated scale and micrometer caliper, respectively. Then the H-type cell was fixed with and without the AEM, respectively. Before testing the resistance of the H-type cells, the connected circular hole must be completely immersed in 3.0 M NaCl (aq.). The resistances R_1 (with the AEM) and R_2 (without the AEM) at room temperature (25 ± 0.5 °C) were collected over the frequency range from 100 mHz to 10 000 Hz. The conductivity (σ) was calculated as follows:

$$\sigma = \frac{4L}{(R_1 - R_2)\Pi D^2} \quad (1)$$

Ion exchange capacity (IEC)

The IEC value of the MTCP-50 AEM was identified by Mohr titration. Typically, a thoroughly dry MTCP-50 sample of about 100 mg in Cl^- form was weighed (W_{dry}) and ion-exchanged in NaCl (1 mol L^{-1}, 60 °C, 24 h). Afterward, it was rinsed with DI water repeatedly. Subsequently, the sample was immersed in Na_2SO_4 (0.5 mol L^{-1}, 60 °C, 24 h) for another ion exchange. Lastly, Na_2SO_4 aq. was collected and titrated with standard $AgNO_3$ aq. (0.1 mol L^{-1}) using K_2CrO_4 as the indicator. The consumed volume of $AgNO_3$ aq. (V_{AgNO_3}) was monitored, and the IEC was calculated as follows:

$$\mathrm{IEC}\ (\mathrm{mmol\ g^{-1}}) = \frac{(V_{AgNO_3} \times C_{AgNO_3})}{W_{dry}} \quad (2)$$

Pore sizes and porosity of HPE

The pore sizes of the HPE membrane were characterized using a capillary flow porometer (CFP-1500AEL, America). The membrane was initially impregnated with the Galwick wetting solution, which has a low surface tension (r = 15.9 dyn cm^{-1}), and N_2 gas was then blown through the membrane. As the gas pressure increased, the Galwick solution in the membrane pores was displaced with the gas, from the largest to the smallest pore, until the membrane was completely dried. The gas flow rate was recorded as a function of the gas pressure to calculate the pore diameter (D_p) of the membrane using the Washburn equation:

$$D_p = \frac{4r\cos\theta}{\Delta p} \quad (3)$$

where θ is the contact angle of the wetting agent and Δp is the differential pressure.[26]

The porosity of the HPE membrane was quantified using the gravimetric method.[26] The support membrane (3 × 3 cm^2) was soaked in EtOH for 3 h, and residual EtOH was then removed using tissue paper. After measuring the dry (W_{dry}) and wet (W_{wet}) weights of the HPE membrane, its overall porosity (ε) was calculated using the following equation:

$$\varepsilon = \frac{(W_{wet} - W_{dry})/\rho_w}{(W_{wet} - W_{dry})/\rho_w + W_{dry}/\rho_m} \times 100\% \quad (4)$$

where ρ_w and ρ_m are the densities of EtOH (0.79 g cm^{-3}) and HPE (0.96 g cm^{-3}), respectively.

Water uptake (WU) and swelling ratio (SR)

The WU and swelling ratio SR of the MTCP-50 membrane were measured in Cl^- form. Weight and length of dry MTCP-50 samples in Cl^- form were recorded (W_{dry}, L_{dry}). Then, the MTCP-50 samples were immersed in DI water for 24 h at different temperatures. The wet weight and length (W_{wet}, L_{wet}) of MTCP-50 samples were measured after wiping the excess surface water. Average values were obtained from the results of at least three tested samples. The WU and SR were finally calculated from the following equations:

$$\text{Water uptake } (\%) = \frac{W_{wet} - W_{dry}}{W_{dry}} \times 100\% \quad (5)$$

$$\text{Swelling ratio } (\%) = \frac{L_{wet} - L_{dry}}{L_{dry}} \times 100\% \quad (6)$$

Mechanical properties

The mechanical properties (tensile strength and elongation at break) of the membranes were measured using a universal tensile testing machine (UTM6104, China). The mechanical properties of the membranes in their wet state were characterized as follows: the membrane was immersed in DI water for 24 h, and residual DI water was subsequently removed using tissue paper. To obtain its strain–stress curve, the wet membrane (length × width = 100 mm × 6 mm) was loaded into the UTM equipment with an initial gauge length of 25 mm and stretched at a constant speed of 50 mm min^{-1}. Average values were obtained from the results of at least three tested samples.

Single cells and 52-stack cell tests

Single cells (RFBS Technologies, Suqian Shidai Energy Storage, China) were assembled (Fig. S1†) using 50 mL of 1.5 M TEMPTMA catholyte and 55 mL of 1.5 M MV anolyte in an Ar environment. The fundamental electrode reactions of TEMPTMA (positive electrolyte) and MV (negative electrolyte) are shown in Fig. S2.† The single cells were operated at a controlled temperature of 23 ± 1 °C. Two peristaltic pumps (Kamoer DIPump550) circulated the electrolytes at a flow rate of 35 mL min^{-1} from polypropylene reservoirs through polyvinyl chloride hoses into a serpentine flow field across a 50 cm^2 active membrane area. Two carbon felt electrodes (Jingu, China, nominal thickness 4 mm, active area 50 cm^2) were positioned on opposite sides of the membrane and compressed to 80% of their original thickness. The assembly process for the CM (Fig. S3†) is as follows: the MTCP-50 AEM was first cut into a square of 10 × 10 cm and then immersed in 1.0 M NaCl (aq.) for at least 24 hours before use. Meanwhile, the HPE membrane was also cut into a square of 10 cm × 10 cm, wetted with DI water, and then assembled between the MTCP-50 AEM and the negative carbon felt electrode.

52-stack cells (RFBS Technologies, Suqian Shidai Energy Storage, China) were assembled (Fig. S4†) using 60 L of 1.5 M TEMPTMA catholyte and 66 L of 1.5 M MV anolyte, all within an Ar environment. The 52-stack cells were operated at 25 ± 2 °C, and two magnetic pumps (DATTO 1.1 Kw) circulated the electrolyte at a rate of 30 L min^{-1} from polypropylene reservoirs through polyvinyl chloride hard pipes into a serpentine flow field across an active membrane area of 830 cm^2. Two carbon felt electrodes (Jingu, China, nominal thickness 4 mm, active area 830 cm^2) were placed on opposing sides of the membrane and compressed to 80% of their original thickness. The MTCP-50 AEMs were initially shaped into rectangles of 400 × 380 cm and then immersed in 1.0 M NaCl (aq.) for at least 24 hours before use. The HPE membranes were also shaped into rectangles of 400 × 380 cm and assembled between the AEM and the negative carbon felt electrode.

For the cell tests, a 1.5 V upper cut-off voltage and a 0.9 V lower cut-off voltage were set for each unit cell. The long-term cycling test was performed at a power density of 66 mW cm^{-2}, while other power tests were carried out at varied power densities of 88 and 110 mW cm^{-2}. Moreover, during the single cell charging process, a constant power charge was applied up to 1.5 V, followed by a constant voltage charge until the current density decreased to 10 mA cm^{-2}. The discharging process involved a constant power discharge down to 0.9 V.

Discussion on the safety and environmental implications

While MV is known to exhibit toxicity if ingested or improperly handled, its environmental impact is mitigated by its rapid degradation in soil and low persistence in ecosystems.[27–29] Compared to other redox-active materials such as vanadium, MV is non-volatile under normal operating conditions, significantly reducing the risk of inhalation exposure.[30,31] To address safety concerns, standardized protocols for handling hazardous materials can be effectively implemented in large-scale battery systems. These measures include the use of protective equipment, proper containment, and rigorous training for personnel. By adopting these practices, the risks associated with MV can be effectively managed, enabling its safe use in advanced energy storage applications.

Results and discussion

Structure and physicochemical properties of HPE

The HPE membrane is characterized by its thinness (7 μm) and high tenacity, particularly notable for its high porosity, with an overall porosity of 44 ± 2% and a pore size of 37 ± 2 nm (Fig. 1(a) and S5†). The combination of high tenacity and nanosized pores effectively restricts electrolyte crossover, while its porous and thin structure reduces mass transport resistance across the HPE membrane.[32,33] Moreover, PE was hydrophilized by ethylene vinyl alcohol (EVOH) modification to enhance its wettability with aqueous electrolytes, similar to the process reported by Choi *et al.*[25] The hydrophobic ethylene units of EVOH form strong hydrophobic interactions with the PE surface, whereas the hydrophilic vinyl alcohol groups are oriented outward, thereby enhancing the hydrophilicity of PE.[34,35]

Structure and physicochemical properties of MTCP-50

The synthesis of the MTCP-50 polymer, production of the polymer solution, and pilot-scale manufacturing of the MTCP-

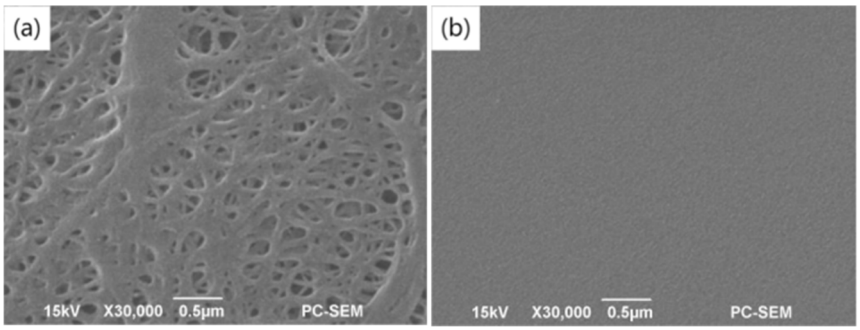

Fig. 1 Scanning electron microscopy (SEM) surface images of the (a) HPE membrane and (b) MTCP-50 AEM. Scale bar: 0.5 μm.

Table 1 The tensile strength and elongation at break of the MTCP-50 AEM with various thicknesses

Membranes	Thickness (μm)	Tensile strength (MPa)	Elongation at break (%)
MTCP-50	40	45 (±1.5)	33 (±1)
MTCP-50	50	52 (±2)	36 (±2)
MTCP-50	60	61 (±2)	40 (±2)

50 AEM with the IEC (1.65 mmol g^{-1}) was performed using the method described by Song *et al.*[17] To prevent visible defects and ensure suitable strength for application, the thickness of the MTCP-50 AEM was set at 60 μm. The MTCP-50 AEM displays a dense surface morphology (Fig. 1(b)), indicative of a flawless membrane. Furthermore, as demonstrated in Table 1, the tensile strength and elongation at break of the MTCP-50 AEM gradually weaken as the thickness decreases. Notably, even at a thickness of 60 μm, the membrane exhibits a relatively low tensile strength of approximately 61 ± 2 MPa. Furthermore, the elongation at break is limited to 40%, which constitutes only 33% of the value observed in the commercial AEM (FAA50).[24] Additionally, MTCP-50 demonstrates a water uptake of 33% and a swelling ratio of 5% at 25 °C (Fig. S6†). This behavior is attributed to the presence of large, highly uniform voids and well-ordered ionic domains, which facilitate the even dispersion of water molecules.[17]

Neutral aqueous organic redox flow battery performance

In this work, we prioritize investigating the MTCP-50 AEM in a 52-stack cell configuration with the active CM area scaled up to 830 cm^2 per piece. Prior to connecting the reservoirs, an internal gas leakage test was performed. For the standard operation of the 52-stack cell, the pressure difference between the positive and negative electrodes is less than 0.2 bar. During the test, only the positive half-cell side is connected to the pressure line, while the negative half-cell side is connected to a gas collection unit. Normally, the stack is pressurized under 0.2 bar for 10 minutes, and the internal gas leakage rate is approximately 0.2 mL s^{-1}. The possible reason for the leakage is the large pores in the MTCP-50 AEM, a flaw resulting from the membrane's detachment from the PET substrate as depicted in Fig. S7.† Furthermore, Fig. 2(a) and (b) show the discharge capacity, coulombic efficiency (CE) and energy efficiency (EE) of the tested stacked cell recorded at a power density of 66 mW cm^{-2} (2848 W) over time. During a 200-hour cycling test, the CE gradually decreases from 99.3% to 95%, showing instability in the end; similarly, the EE gradually decreases from 81% to 72% with the discharge capacity fading at a rate of about 0.26% per hour. Upon disassembling the stack, the MTCP-50 AEMs exhibit signs of mild to severe corrosion, with some membranes severely damaged (Fig. S8a and b†). This corrosion is identified as the primary reason for stack failure. As mentioned above, the mechanical strength of the MTCP-50 AEM is compromised due to large pores that develop during the membrane's detachment from the PET substrate. In regions with these flaws, crossover of positive and negative electrolytes occurs, leading to over-voltage and subsequent chlorine evolution, which ultimately induces membrane corrosion. To validate this hypothesis, we designed a single cell featuring a membrane with a 0.5 mm round hole. Following approximately 15 hours of operation, both the membrane and the blue seal membrane, as depicted in Fig. S8c and d,† exhibit corrosion similar to that observed in the disassembled stack, with the inside of the blue seal membrane appearing bleached. Conversely, the single cell featuring a CM with the MTCP-50 AEM containing one 0.5 mm round hole shows no noticeable signs of corrosion after about 90 hours of operation, as evidenced in Fig. S8e and f.† These findings clearly demonstrate that the large pores are a primary contributor to the failure of the stack. The oxidative stability of the MTCP-50 membrane material has been previously investigated by Song *et al.* Their work demonstrated that the MTCP-50 AEM sample exhibits a high weight retention of 97.74% after immersion in Fenton's reagent for 24 hours, which is comparable to that of Nafion. Additionally, the MTCP-50 samples remained transparent and maintained mechanical integrity, confirming their excellent oxidative stability.[17] To further evaluate the oxidative stability of the MTCP-50 membrane in the TEMPTMA catholyte, we conducted mechanical tests. The MTCP-50 membranes were immersed in TEMPTMA catholyte (1.5 M, 50 °C, under a 100% state of charge) for 90 days, and the mechanical properties of the membranes were characterized at different soaking intervals. As shown in Fig. S9,† the MTCP-50 membrane retained excellent mechanical strength, with 96% retention of tensile strength and 95% retention of elongation at break after 90 days of oxidative testing. These results suggest that the MTCP-50 AEM is sufficiently mechanically robust for long-term applications in AORFBs.

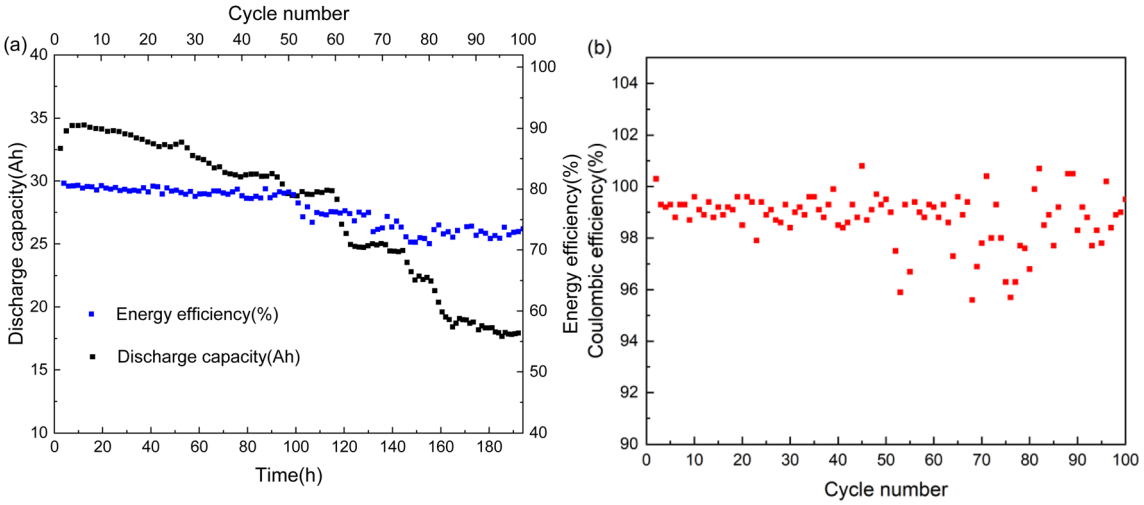

Fig. 2 (a) The discharge capacity, EE and (b) CE of the 52-stack cell assembled with the MTCP-50 AEMs.

The long-term cycling stability of the TEMPTMA and MV-based AORFB system using the MTCP-50 AEM has been evidenced in aqueous solutions at a concentration of 1.5 M. In this work, to compare the cell performance of the CM membrane with the MTCP-50 AEM, a single cell with a 50 cm^2 active CM area was assessed. Fig. 3(a) illustrates the discharge capacity, CE and EE results for a single cell recorded at a power density of 66 mW cm^{-2} (3.3 W). During the 1500-hour cycling test with a 1.5 M electrolyte, the cell maintains a relatively stable level of both CE (~100%) and EE (~80%). The single cell exhibits excellent cycling performance, with the discharge capacity fading at a rate of about 0.0034% per hour over 1100 cycles (equivalent to a capacity retention of 99.9966% per hour), which is similar to the findings reported by Song *et al.*[17] To address potential compatibility issues arising from the dual-membrane design, the single cell was assembled with two carbon felt electrodes positioned on opposite sides of the membrane and compressed to 80% of their original thickness. This compression provides a pressure of 0.25 atm, ensuring proper contact between the membranes and electrodes while maintaining structural integrity. The median discharge voltage of the single cell during the 1500-hour test, as shown in Fig. S10,† demonstrates stable ionic conductivity of the CM in the electrolyte. After the 1500-hour cycling test, the HPE membrane remains completely immersed in water (Fig. S11†), indicating its exceptional hydrophilic stability in the electrolyte. Moreover, we compare the influence of the MTCP-50 AEM and CM on the EE in the single cell, showing results at varied power densities of 66, 88 and 110 mW cm^{-2} (Fig. 3(b)). Due to the highly porous and thin structure of the PE hydrophilized by ethylene vinyl alcohol (EVOH) modification, which reduces mass transport resistance across and permits ion transport through its pores,[32,33] there is only a small difference in EE between the MTCP-50 AEM and the CM.

Furthermore, we investigate a CM with a large area (830 cm^2) as a single piece and 52 pieces used in a stacked cell. After

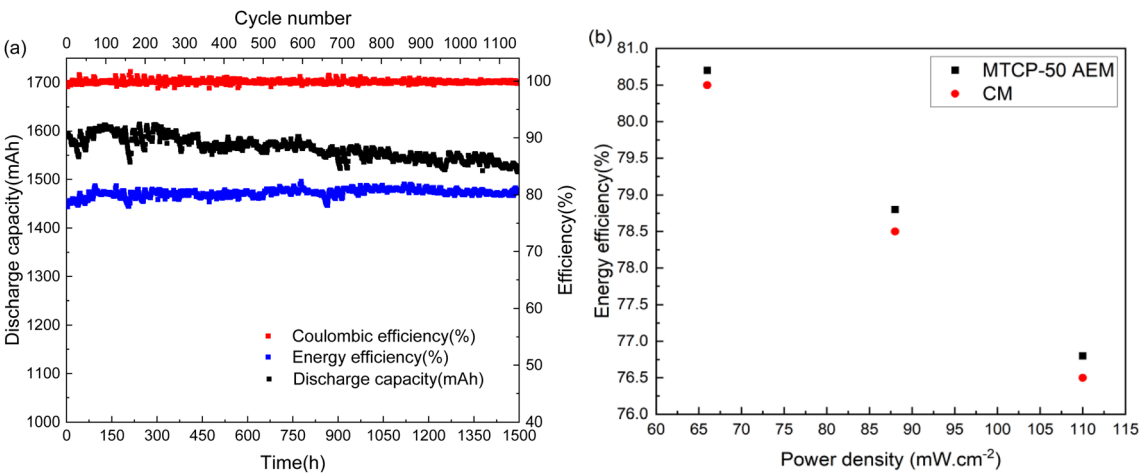

Fig. 3 (a) The electrochemical performance of the single cell assembled with the CM. (b) The EE for the MTCP-50 AEM and CM at power densities of 66, 88 and 110 mW cm^{-2} in a single cell.

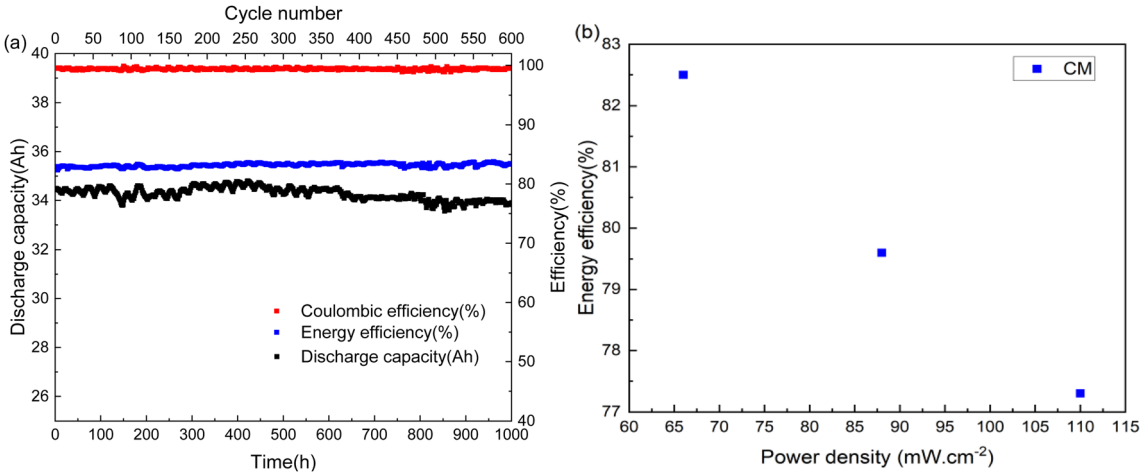

Fig. 4 (a) The electrochemical performance of the 52-stack cell assembled with the CM. (b) The EE for the 52-stack cell assembled with the CM at power densities of 66, 88 and 110 mW cm^{-2}.

assembling the stack, an internal gas leakage test was performed before connecting the reservoirs to the stack setup with the same method described previously. Due to the HPE membrane's small pore size (37 ± 2 nm), the normal internal gas leakage rate of the stack is lower than 0.002 mL s^{-1}. The discharge capacity, CE and EE of the stacked cell tested at a power density of 66 mW cm^{-2} (2848 W) over time are shown in Fig. 4(a). In a 1000-hour cycling test using a 1.5 M electrolyte, the stacked cell retains high CE (~99.4%) and EE (~82.5%) values without attenuation. Furthermore, it demonstrates excellent cycling performance, with the discharge capacity fading at a rate of about 0.0027% per hour over 1100 cycles, which is similar to the performance of the single cell with the CM. Comparative analyses of the MTCP-50 AEM before and after 1000 hours of cycling using ^{1}H NMR spectroscopy and FT-IR spectroscopy are shown in Fig. S12.† Both spectroscopic techniques reveal no significant group degradation. The IEC of the MTCP-50 AEM, tested before and after 1000-hour cycles, shows a minimal decrease from 1.65 mmol g^{-1} to 1.62 mmol g^{-1}, a loss of approximately 1.8%. This minor IEC reduction likely results from slight degradation involving ring opening and nucleophilic substitution reactions on the piperidinium cation.[17] Moreover, resistance measurements of the single cell with the CM after 2 and 1000 hours of cycling (under a 50% state of charge) indicate an increase in cell resistance of about 1.2%, suggesting stable ionic conductivity of the CM in the electrolyte, as shown in Fig. S13 (ESI†). Subsequently, we explore the varied power densities of the CM in the stacked cell. As illustrated in Fig. 4(b), the EE is 82.5%, 79.6% and 77.3% at power densities of 66, 88 and 110 mW cm^{-2}, respectively.

Conclusions

In this study, we introduce for the first time a novel CM that integrates an anion exchange membrane (AEM) layer with hydrophilic porous polyethylene (HPE) and its use in aqueous organic redox flow batteries (AORFBs) with a large active area in a single piece. The dense and highly anionic conductive AEM layer effectively prevents electrolyte crossover while promoting anion transport. Additionally, the HPE membrane, characterized by its high tenacity and nanosized pores, restricts electrolyte crossover, and its highly porous and thin structure minimizes mass transport resistance across the HPE membrane. In single-cell applications, the CM exhibits exceptionally stable performance, achieving a capacity retention of 99.9966% per hour. Furthermore, the CM demonstrates long-term stability in a 52-stack cell configuration, maintaining a capacity retention of 99.9973% per hour, thereby ensuring its great potential for commercial viability. In future work, we aim to investigate and develop a CM based on PE substrates, with the goal of reducing costs, significantly enhancing mechanical strength and improving reliability. These advancements will focus on optimizing the membrane's structural and functional properties to meet the demands of scalable energy storage technologies.

Author contributions

C. L. and M. H. contributed equally to this work. C. L. and P. C. conceived this idea and designed the experiments. C. L. and R. H. performed the materials synthesis and electrochemical measurements. C. L. and M. H. conducted the data analysis and wrote the paper. All authors took part in the result discussion and data analysis.

Data availability

The authors declare that data supporting the findings of this study are available within the paper and the ESI.† All other data are available from the lead contact upon reasonable request.

Conflicts of interest

There are no conflicts to declare.

Acknowledgements

The work described in this paper was fully supported by Suqian Shidai Energy Storage Co., Ltd.

References

1 E. Sánchez-Díez, *et al.*, Redox flow batteries: Status and perspective towards sustainable stationary energy storage, *J. Power Sources*, 2021, **481**, 228804.
2 A. Z. Weber, *et al.*, Redox flow batteries: a review, *J. Appl. Electrochem.*, 2011, **41**, 1137–1164.
3 G. L. Soloveichik, Flow Batteries: Current Status and Trends, *Chem. Rev.*, 2015, **115**, 11533–11558.
4 P. Alotto, M. Guarnieri and F. Moro, Redox flow batteries for the storage of renewable energy: A review, *Renew. Sustain. Energy Rev.*, 2014, **29**, 325–335.
5 European Commission, *Communication from the Commission to the European Parliament*, The European Council, The Council, The European Economic And Social Committee And The Committee Of The Regions The European Green Deal, 2019.
6 J. Winsberg, T. Hagemann, T. Janoschka, M. D. Hager and U. S. Schubert, Redox-Flow Batteries: From Metals to Organic Redox-Active Materials, *Angew. Chem., Int. Ed.*, 2017, **56**, 686–711.
7 G. Kear, A. A. Shah and F. C. Walsh, Development of the all-vanadium redox flow battery for energy storage: a review of technological, financial and policy aspects, *Int. J. Energy Res.*, 2012, **36**, 1105–1120.
8 X. Wei, *et al.*, Materials and Systems for Organic Redox Flow Batteries: Status and Challenges, *ACS Energy Lett.*, 2017, **2**, 2187–2204.
9 K. Wedege, E. Dražević, D. Konya and A. Bentien, Organic Redox Species in Aqueous Flow Batteries: Redox Potentials, Chemical Stability and Solubility, *Sci. Rep.*, 2016, **6**, 39101.
10 B. Yang, L. Hoober-Burkhardt, F. Wang, G. K. S. Prakash and S. R. Narayanan, An Inexpensive Aqueous Flow Battery for Large-Scale Electrical Energy Storage Based on Water-Soluble Organic Redox Couples, *J. Electrochem. Soc.*, 2014, **161**, A1371.
11 L. J. Small, H. D. Pratt and T. M. Anderson, Crossover in Membranes for Aqueous Soluble Organic Redox Flow Batteries, *J. Electrochem. Soc.*, 2019, **166**, A2536.
12 M. T. Tsehaye, *et al.*, Anion exchange membranes with high power density and energy efficiency for aqueous organic redox flow batteries, *Electrochim. Acta*, 2023, **438**, 141565.
13 J. Wang, *et al.*, Poly(aryl piperidinium) membranes and ionomers for hydroxide exchange membrane fuel cells, *Nat. Energy*, 2019, **4**, 392–398.
14 N. Chen, *et al.*, Poly(Alkyl-Terphenyl Piperidinium) Ionomers and Membranes with an Outstanding Alkaline-Membrane Fuel-Cell Performance of 2.58 W cm−2, *Angew. Chem., Int. Ed.*, 2021, **60**, 7710–7718.
15 N. Chen, *et al.*, Poly(fluorenyl aryl piperidinium) membranes and ionomers for anion exchange membrane fuel cells, *Nat. Commun.*, 2021, **12**, 2367.
16 X. Wu, N. Chen, H.-A. Klok, Y. M. Lee and X. Hu, Branched Poly(Aryl Piperidinium) Membranes for Anion-Exchange Membrane Fuel Cells, *Angew. Chem.*, 2022, **134**, e202114892.
17 T. Xu, *et al.*, Upscaled production of an ultramicroporous anion-exchange membrane enables long-term operation in electrochemical energy devices, *Nat. Commun.*, 2023, **14**, 2732.
18 X. Che, *et al.*, Porous polybenzimidazole membranes with high ion selectivity for the vanadium redox flow battery, *J. Membr. Sci.*, 2020, **611**, 118359.
19 N. Shi, *et al.*, Acid doped branched poly(biphenyl pyridine) membranes for high temperature proton exchange membrane fuel cells and vanadium redox flow batteries, *Chem. Eng. J.*, 2024, **489**, 151121.
20 M. Rykær Kraglund, *et al.*, Ion-solvating membranes as a new approach towards high rate alkaline electrolyzers, *Energy Environ. Sci.*, 2019, **12**, 3313–3318.
21 R. Varcoe, *et al.*, Anion-exchange membranes in electrochemical energy systems, *Energy Environ. Sci.*, 2014, **7**, 3135–3191.
22 D. Li, *et al.*, Durability of anion exchange membrane water electrolyzers, *Energy Environ. Sci.*, 2021, **14**, 3393–3419.
23 N. Pismenskaya, V. Nikonenko, B. Auclair and G. Pourcelly, Transport of weak-electrolyte anions through anion exchange membranes: Current–voltage characteristics, *J. Membr. Sci.*, 2001, **189**, 129–140.
24 H. Andrew Miller, *et al.*, Green hydrogen from anion exchange membrane water electrolysis: a review of recent developments in critical materials and operating conditions, *Sustainable Energy Fuels*, 2020, **4**, 2114–2133.
25 J. Choi, *et al.*, Thin Film Composite Membranes as a New Category of Alkaline Water Electrolysis Membranes, *Small*, 2023, **19**, 2300825.
26 S. J. Kwon, *et al.*, Fabrication of high performance and durable forward osmosis membranes using mussel-inspired polydopamine-modified polyethylene supports, *J. Membr. Sci.*, 2019, **584**, 89–99.
27 J. B. Weber and S. B. Weed, Adsorption and Desorption of Diquat, Paraquat, and Prometone by Montmorillonitic and Kaolinitic Clay Minerals, *Soil Sci. Soc. Am. J.*, 1968, **32**, 485–487.
28 Z. E. Suntres, Role of antioxidants in paraquat toxicity, *Toxicology*, 2002, **180**, 65–77.
29 R. J. Dinis-Oliveira, *et al.*, Paraquat Poisonings: Mechanisms of Lung Toxicity, Clinical Features, and Treatment, *Crit. Rev. Toxicol.*, 2008, **38**, 13–71.
30 B. Huskinson, *et al.*, A metal-free organic–inorganic aqueous flow battery, *Nature*, 2014, **505**, 195–198.
31 J. Winsberg, T. Hagemann, T. Janoschka, M. D. Hager and U. S. Schubert, Redox-Flow Batteries: From Metals to Organic Redox-Active Materials, *Angew. Chem., Int. Ed.*, 2017, **56**, 686–711.
32 X. Li, Q. Li, W. Fang, R. Wang and W. B. Krantz, Effects of the support on the characteristics and permselectivity of thin film composite membranes, *J. Membr. Sci.*, 2019, **580**, 12–23.
33 H. J. Park, S. Y. Lee, T. K. Lee, H.-J. Kim and Y. M. Lee, N3-butyl imidazolium-based anion exchange membranes

blended with Poly(vinyl alcohol) for alkaline water electrolysis, *J. Membr. Sci.*, 2020, **611**, 118355.

34 D. Y. Kim, H. Park, Y.-I. Park and J.-H. Lee, Polyvinyl alcohol hydrogel-supported forward osmosis membranes with high performance and excellent pH stability, *J. Ind. Eng. Chem.*, 2021, **99**, 246–255.

35 K. Nakamae, T. Miyata and T. Matsumoto, Surface characterization of ethylene-vinyl alcohol copolymer membranes prepared under various conditions, *J. Membr. Sci.*, 1992, **75**, 163–170.

